



## Research paper

Heterogeneous oxidation of elemental mercury vapor over RuO<sub>2</sub>/rutile TiO<sub>2</sub> catalyst for mercury emissions control

Zhouyang Liu, Vishnu Sriram, Joo-Youp Lee\*

Chemical Engineering Program, Department of Biomedical, Chemical, and Environmental Engineering, University of Cincinnati, Cincinnati, OH, 45221-0012, United States

## ARTICLE INFO

## Article history:

Received 10 September 2016

Received in revised form 30 January 2017

Accepted 6 February 2017

Available online 7 February 2017

## Keywords:

Mercury oxidation

Ruthenium oxide

Rutile titanium dioxide

Coal-fired power plants

Flue gas

## ABSTRACT

The catalytic oxidation of elemental mercury (Hg(0)) vapor is an effective way to enhance mercury removal from coal-fired power plants. RuO<sub>2</sub> catalyst was found to be an excellent Hg(0) oxidation catalyst. When rutile TiO<sub>2</sub> was used as the catalyst support, RuO<sub>2</sub> formed well dispersed nano-layers due to the very similar crystal structures of RuO<sub>2</sub> and rutile TiO<sub>2</sub>, giving higher Hg(0) oxidation activity over anatase TiO<sub>2</sub> support. The RuO<sub>2</sub>/rutile TiO<sub>2</sub> catalyst can be used at the tail end section of the selective catalytic reduction (SCR) unit for Hg(0) oxidation. It showed good Hg(0) oxidation performance under sub-bituminous and lignite coal simulated flue gas conditions with low concentration of HCl or HBr gas. The RuO<sub>2</sub>/rutile TiO<sub>2</sub> catalyst also showed excellent resistance to SO<sub>2</sub> under bituminous coal simulated flue gas, maintaining higher than 90% Hg(0) oxidation with up to 2,000 ppmv SO<sub>2</sub> present. The oxidized mercury in a form of HgCl<sub>2</sub> has a high solubility in water and can be easily captured by other air pollution control systems such as wet scrubbers in coal-fired power plants.

© 2017 Elsevier B.V. All rights reserved.

## 1. Introduction

Coal naturally contains small amounts of mercury (around 0.1–0.2 ppm by weight) and they will be released into the flue gas after the combustion [1,2]. It is estimated that around 53 tons of mercury are emitted from coal-fired power plants each year in the United States, accounting for around 50% of emissions from all anthropogenic mercury sources [3]. Mercury has long been recognized as a highly toxic and persistent pollutant. The 1990 Amendments to the Clean Air Act listed mercury as one of the most toxic pollutants among 188 hazardous air pollutants. In 2012, the U.S. EPA finalized the air toxics standards for coal- and oil-fired electric generating units also known as the Mercury Air Toxics Standards (MATS) [4]. Prior to the MATS rule in 2011, EPA finalized the Cross-State Air Pollution Rule (CSAPR), replacing the EPA's earlier Clean Air Interstate Rule (CAIR) from 2005 [5]. CSAPR further reduces NO<sub>x</sub> and SO<sub>2</sub> emissions from power plants in 28 states, and as a result, additional installations of flue gas desulfurization (FGD) and NO<sub>x</sub> control systems such as a selective catalytic reduction (SCR) unit are expected.

After combustion, mercury is released and exists in three forms in coal-fired power plants flue gas: oxidized mercury (Hg(2+)), particulate mercury (Hg(p)), and elementary mercury (Hg(0)). The first two forms are readily removed with existing air pollution control systems such as fabric filter (FF), electrostatic precipitators (ESP), and wet FGD [6–8]. Hg(0) is most difficult to remove due to its high volatility, low reactivity and low solubility. Currently, sorbent injection (raw or modified activated carbon), halogen salt (e.g. CaBr<sub>2</sub>) addition to the boiler and SCR optimization are commercially available mercury emissions control technologies [9]. Because of the vastly different coal properties and power plant configurations, there is no universal mercury control solution that fits all scenarios, and combinations of control methods are often needed. Activated carbon injection is the most well-studied and mature technology, but the cost is high. The U.S. Department of Energy estimates that the costs for sorbent injection to achieve 90 percent removal are estimated to be between \$25,000 and \$70,000 per pound of mercury removed [10]. Also, activated carbon sorption capacity is significantly reduced under high sulfur coal conditions [11]. Due to the increasing number of FGD units resulted from recent EPA rules, oxidizing elemental mercury using SCR or other catalysts, followed by oxidized mercury capture in wet FGD is a viable option. Noble metal-based catalysts such as gold, platinum and palladium have been studied as Hg(0) oxidation catalysts [12,13]. Various metal oxide-based Hg(0) oxidation

\* Corresponding author.

E-mail addresses: [liuzy@mail.uc.edu](mailto:liuzy@mail.uc.edu) (Z. Liu), [sriramvu@mail.uc.edu](mailto:sriramvu@mail.uc.edu) (V. Sriram), [jooyoup@gmail.com](mailto:jooyoup@gmail.com), [joo.lee@uc.edu](mailto:joo.lee@uc.edu) (J.-Y. Lee).

catalysts, SCR and modified SCR catalysts have also been studied for Hg(0) oxidation [14–22]. Due to the oxygen storing and releasing property of CeO<sub>2</sub>, its application in Hg(0) oxidation and adsorption in flue gas has been studied in recent years. Nanostructured CeO<sub>2</sub>–MnO<sub>x</sub> catalyst and CeO<sub>2</sub>-based solid solutions showed good Hg(0) removal performance from increased oxygen vacancies and catalytic activity [23,24]. CeO<sub>2</sub>–TiO<sub>2</sub> and CeO<sub>2</sub> modified MnO<sub>x</sub>–TiO<sub>2</sub> were reported to have Hg(0) adsorption capability [25,26]. CeO<sub>2</sub> was also reported to have a promotional effect for Hg(0) oxidation in a modified SCR catalyst [27]. But, most of them only showed limited Hg(0) oxidation performances at low HCl concentrations of typical flue gases from lignite and sub-bituminous coals. Also, these catalysts are susceptible to SO<sub>2</sub> and NH<sub>3</sub> inhibition and showed degraded performances under high sulfur bituminous coal flue gas conditions (e.g., 2,000 ppmv SO<sub>2</sub>). For low rank sub-bituminous and lignite coals with low chlorine (typically with HCl <10 ppmv in the flue gas), additional halogen is usually needed to achieve satisfactory Hg(0) oxidation. Currently, halogen salts such as CaCl<sub>2</sub> or CaBr<sub>2</sub> injection to the boiler to enhance Hg(0) oxidation is one of the most widely used methods [28]. In the absence of any catalyst (either SCR or Hg(0) oxidation catalyst), high injection rate of the halogen salts is required, and it was reported to cause corrosion problems especially in the air-preheater [29,30]. A combination of halogen salts addition and Hg(0) oxidation catalysts could be an economical and feasible solution [31].

Recently, RuO<sub>2</sub>-based catalysts were developed for the Deacon reaction for the oxidation of HCl by O<sub>2</sub> to produce Cl<sub>2</sub> [32,33]. It was also found that many Deacon reaction catalysts can also catalyze the Hg(0) oxidation reaction by utilizing HCl gas [17]. In our previous study, oxidized mercury species obtained from the RuO<sub>2</sub>/rutile TiO<sub>2</sub> catalyst were analyzed using X-ray Absorption Near-Edge Structure (XANES) spectroscopy [34]. A major focus of the study was to identify and quantify the oxidized mercury species generated as a result of the reaction of Hg(0) vapor over the catalyst under different simulated flue gas conditions. In the presence of HCl or HBr gas with O<sub>2</sub> gas, HgCl<sub>2</sub> or HgBr<sub>2</sub> was found to be a major oxidized mercury species. HgCl<sub>2</sub> and HgBr<sub>2</sub> have high solubility in water, and can be easily scrubbed by wet FGD scrubbers in coal-fired power plants. In this study, the performances of the RuO<sub>2</sub>/rutile TiO<sub>2</sub> catalyst were investigated in terms of different TiO<sub>2</sub> phases, synthesis methods and gas and temperature conditions.

## 2. Experimental

### 2.1. Catalyst synthesis

RuO<sub>2</sub>/TiO<sub>2</sub> catalysts were synthesized using RuCl<sub>3</sub> (Sigma-Aldrich) as the precursor. Commercial anatase- and rutile-phase TiO<sub>2</sub> were obtained from Cristal Co. and Sakai Chemical, respectively. Three synthesis methods were used for RuO<sub>2</sub>/TiO<sub>2</sub> catalysts, and the procedures are summarized below.

Wetness incipient (WI) method: RuCl<sub>3</sub> was dissolved in a small amount of water (around 0.9 mL per gram of TiO<sub>2</sub>) and the solution was added to dry TiO<sub>2</sub> powder. After thorough mixing, the catalyst was dried at room temperature for 12 h and calcined at 400 °C in air for 3 h.

Deposition-precipitation (DP) method: TiO<sub>2</sub> powder was added to water (25 mL water per gram of TiO<sub>2</sub> powder) under vigorous stirring. Then RuCl<sub>3</sub> was added and the slurry was heated to 45 °C. A 1 M Na<sub>2</sub>CO<sub>3</sub> solution was added dropwise until pH > 10 to precipitate all RuCl<sub>3</sub> [35,36]. The catalyst was then filtered, washed thoroughly, dried at room temperature for 12 h and calcined at 400 °C in air for 3 h.

Strong electrostatic adsorption (SEA) method: TiO<sub>2</sub> powder was added to water (25 mL water per gram of TiO<sub>2</sub> powder) under vig-

orous stirring and an ammonium hydroxide solution was added until pH reached 11.5. RuCl<sub>3</sub> was then added and stirred for 3 h [37]. This method utilizes electrostatic charges for adsorption of active metals onto substrate. The point of zero charge (PZC) for TiO<sub>2</sub> in the aqueous phase is around 6. When the pH of a solution is greater than that the PZC (i.e. ~6), TiO<sub>2</sub> surface is negatively charged. Ru(NH<sub>3</sub>)<sub>6</sub><sup>3+</sup> formed from RuCl<sub>3</sub> and ammonium hydroxide is positively charged and adsorbs onto the TiO<sub>2</sub> surface. The catalyst was then filtered, washed thoroughly, dried at room temperature for 12 h and calcined at 400 °C in air for 3 h.

SCR catalyst with 1 wt% V<sub>2</sub>O<sub>5</sub> loading was synthesized by following a procedure below: 12 g of anatase TiO<sub>2</sub> powder (DT-58, Cristal, containing 9.1 wt% tungsten and 10.5 wt% silica), 0.3 g of methylcellulose (Sigma-Aldrich) and 0.24 g of glass fiber (Fibre Glast) were dry mixed for 10 min. 0.138 g of NH<sub>4</sub>VO<sub>3</sub> (Sigma-Aldrich) dissolved in 11 mL of 1 M oxalic acid (Sigma-Aldrich) was added to the above powders and the dough was kneaded for 10 min for uniform mixing. All the catalysts were extruded into 1 mm (diameter) × 5 mm (length) cylindrical pellets, and were dried in air at room temperature, followed by calcination at 500 °C in air for 3 h.

### 2.2. Characterization

The BET surface area, pore volume and pore diameter were measured by an accelerated surface area and porosimetry system (ASAP 2020, Micromeritics). The high-resolution transmission electron microscopy (HR-TEM) experiments were conducted using JEOL 2010F equipped with a field emission gun operating at 200 keV with a point-to-point resolution of 0.19 nm. Energy-dispersive X-ray spectroscopy was conducted using the same instrument with an Oxford INCA EDX detector. The X-ray diffraction (XRD) measurement was carried out with an X'Pert Pro MPD X-ray diffractometer under Cu K $\alpha$  radiation (wavelength = 1.5406 Å). The powdered samples were loaded in an aluminum holder with a depth of 1 mm. The scanning range was from 10 to 60° (2 $\theta$ ) with a step size of 0.02° and a time step of 0.5 s. Ruthenium K edge (22,117 eV) X-ray absorption fine structure (XAFS) spectra were collected using the 9-BM-B beamline (Sector 9) at the Advanced Photon Source (APS) at Argonne National Laboratory (ANL, Chicago, IL). A Si (111) monochromator was used, with energy resolution ( $\Delta E/E$ ) of approximately  $1.4 \times 10^{-4}$ . Energy calibration was monitored by measuring the absorption through a reference ruthenium foil simultaneously with the absorption through the samples. Samples were loaded onto Teflon holder between two layers of Kapton tapes and measured in transmission mode. A RuO<sub>2</sub> standard was obtained from Sigma-Aldrich. A spent RuO<sub>2</sub>/rutile TiO<sub>2</sub> catalyst sample treated after 48 h of Hg(0) oxidation under a simulated flue gas (containing 15 ppbv Hg(0), 10 ppmv HCl, 5 ppmv NH<sub>3</sub>, 5 ppmv NO, 200 ppmv SO<sub>2</sub>, 3%(v) O<sub>2</sub>, 10%(v) H<sub>2</sub>O, 12%(v) CO<sub>2</sub> balanced with N<sub>2</sub>) at 350 °C was also examined for XRD and XAFS analyses. At least five scans were collected for each sample in order to improve the signal-to-noise ratio. XAFS data collected were analyzed using the Athena software package [38].

### 2.3. Performance tests

The performances of RuO<sub>2</sub>/TiO<sub>2</sub> catalysts were tested using a fixed-bed reactor system. A schematic of the apparatus is shown in Fig. 1. Elemental mercury (Hg(0)) vapor was generated using a permeation oven (Dynacalibrator, VICI Metronics) using N<sub>2</sub> as a carrier gas and the inlet Hg(0) vapor concentration was 10–15 ppbv. Water vapor was generated using a bubbler. All the other simulated flue gas components were prepared from compressed gas cylinders (Wright Brothers, Inc.) and the concentrations were controlled by mass flow controllers. The catalysts with ruthenium metal loading of 0.2–1 wt% (in terms of Ru) were used for the performance tests.

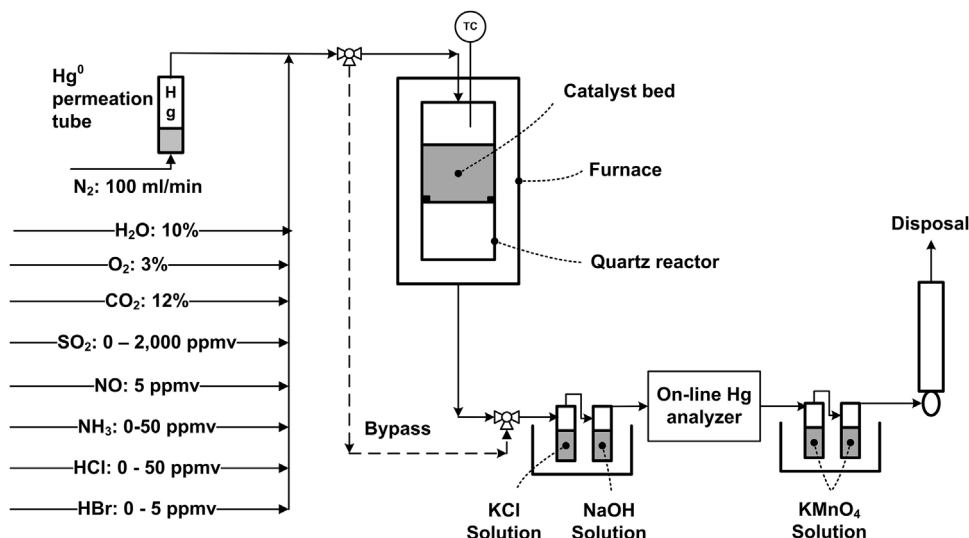


Fig. 1. A schematic of the experimental set-up for the catalysts performance test.

The catalysts in the form of extruded pellets ( $1\text{ mm} \times 5\text{ mm} (\text{D} \times \text{L})$ ) were placed inside a vertically mounted quartz reactor with a diameter of 16 mm and the temperature was maintained at  $350^\circ\text{C}$  in a tubular furnace. For performance tests under simulated flue gas conditions, 1.7 g of catalysts were used and the catalyst bed height was around 15 mm. The temperature was chosen to approximate the temperature at the tail end of the SCR unit at coal-fired power plants. The total flow rate of the simulated flue gas was 1 L/min with a gas hourly space velocity  $40,000\text{ h}^{-1}$  (about 10 times higher than typical commercial SCR units). It was confirmed that  $\text{Hg}(0)$  oxidation under the simulated flue gas conditions was negligible in the absence of the catalysts. Each performance test was conducted for 6–24 h after making sure that the system was stabilized. The  $\text{Hg}(0)$  oxidation efficiency and oxidation rate were calculated by measuring the concentrations across the reactor bed using the following Eqs. (1) and (2):

$$\text{Hg}(0) \text{ oxidation efficiency} = \frac{\text{Hg}(0)_{\text{in}} - \text{Hg}(0)_{\text{out}}}{\text{Hg}(0)_{\text{in}}} \times 100\% \quad (1)$$

$$\text{Hg}(0) \text{ oxidation rate} = \frac{\text{Hg}(0)_{\text{in}} - \text{Hg}(0)_{\text{out}}}{\text{time}} \quad (2)$$

$\text{SO}_3$  generated from the catalyst under a simulated flue gas containing high  $\text{SO}_2$  concentration was measured using U.S. EPA Method 8 [39]. Two impinger solutions containing 80% (v) isopropanol in water and 3% (v)  $\text{H}_2\text{O}_2$  in water in series were used to capture  $\text{SO}_3$  and  $\text{SO}_2$ , respectively. Then both fractions were measured separately by the barium-thorin titration method.

### 3. Results and discussion

#### 3.1. Catalysts characterization

##### 3.1.1. TEM

In this study, two types of  $\text{TiO}_2$  support (anatase and rutile) and three synthesis methods (WI, DP, SEA) were used. The TEM images of these  $\text{RuO}_2/\text{TiO}_2$  catalysts with 1% (wt) Ru loading were taken to obtain the information on the morphology of the metal oxides. When anatase  $\text{TiO}_2$  was used,  $\text{RuO}_2$  formed large aggregates ranging from 50 to 100 nm for all three synthesis methods as shown in Fig. 2-b, 2-c and 2-d.  $\text{RuO}_2$  particles were much bigger than anatase  $\text{TiO}_2$  particles and the metal dispersion was poor. EDX indicated that  $\text{RuO}_2$  mainly existed as large aggregates and there was only a very small amount present on the anatase  $\text{TiO}_2$  surface. The mor-

Table 1

BET surface area, pore volume and average pore diameter measurements for synthesized  $\text{RuO}_2/\text{rutile TiO}_2$  and SCR catalysts.

Catalyst	BET surface area ( $\text{m}^2/\text{g}$ )	Pore volume ( $\text{cm}^3/\text{g}$ )	Average pore diameter ( $\text{\AA}$ )
Rutile $\text{TiO}_2$	72	0.38	202
0.2% Ru loading	69	0.31	194
0.5% Ru loading	66	0.28	184
1% Ru loading	64	0.28	186
Synthesized SCR	95	0.29	126
Commercial SCR [36–39]	61–120	0.17–0.29	103–151

phology of  $\text{RuO}_2$  changed significantly when rutile  $\text{TiO}_2$  was used as a support. Under low resolution TEM, no  $\text{RuO}_2$  particle could be found from all the three different synthesis methods. However, EDX proved that  $\text{RuO}_2$  was present on the surface. Fig. 2-e and 2-f are rutile  $\text{TiO}_2$  and  $\text{RuO}_2/\text{rutile TiO}_2$  (prepared by WI) samples, respectively. The lighter spots on the  $\text{TiO}_2$  surface are holes and pores. In order to confirm the morphology of  $\text{RuO}_2$ , the catalysts were also examined by high resolution TEM. Rutile  $\text{TiO}_2$  itself had clean surfaces (Fig. 2-g). After doping with ruthenium, it was found that  $\text{RuO}_2$  formed a thin uniform coating on rutile  $\text{TiO}_2$  surface with a thickness of 1–2 nm as shown in Fig. 2-h. No noticeable difference on  $\text{RuO}_2$  morphology was observed among the three different synthesis methods.

For  $\text{RuO}_2$  as a Deacon catalyst, Seki also reported the formation of a nano-sized layer of  $\text{RuO}_2$  crystals on rutile  $\text{TiO}_2$  [32]. Xiang et al. observed the transformation from  $\text{RuO}_2$  particles to epitaxial layer during Deacon reaction [40]. Both  $\text{RuO}_2$  and rutile  $\text{TiO}_2$  have the same body-centered tetragonal structure with very similar lattice constants:  $\text{RuO}_2$  with  $a=b=0.46\text{ nm}$ ,  $c=0.30\text{ nm}$  and rutile  $\text{TiO}_2$  with  $a=b=0.45\text{ nm}$ ,  $c=0.31\text{ nm}$ . This similarity makes it easier for  $\text{RuO}_2$  to deposit onto rutile  $\text{TiO}_2$  surface and to form highly dispersed nano-layers [40,41]. These results suggest that lattice matching between  $\text{RuO}_2$  and rutile  $\text{TiO}_2$  be a stronger driving force for the dispersion of  $\text{RuO}_2$  than the effects of different catalyst synthesis methods.

##### 3.1.2. BET

The BET surface area, pore volume and average pore diameter of  $\text{RuO}_2/\text{rutile TiO}_2$  WI catalysts with different metal loadings and synthesized SCR catalyst were measured and listed in Table 1. The BET surface area, pore volume and average pore diameter decreased from  $72$  to  $64\text{ m}^2/\text{g}$ ,  $0.38\text{--}0.28\text{ cm}^3/\text{g}$  and  $202\text{--}186\text{ \AA}$ , respectively,

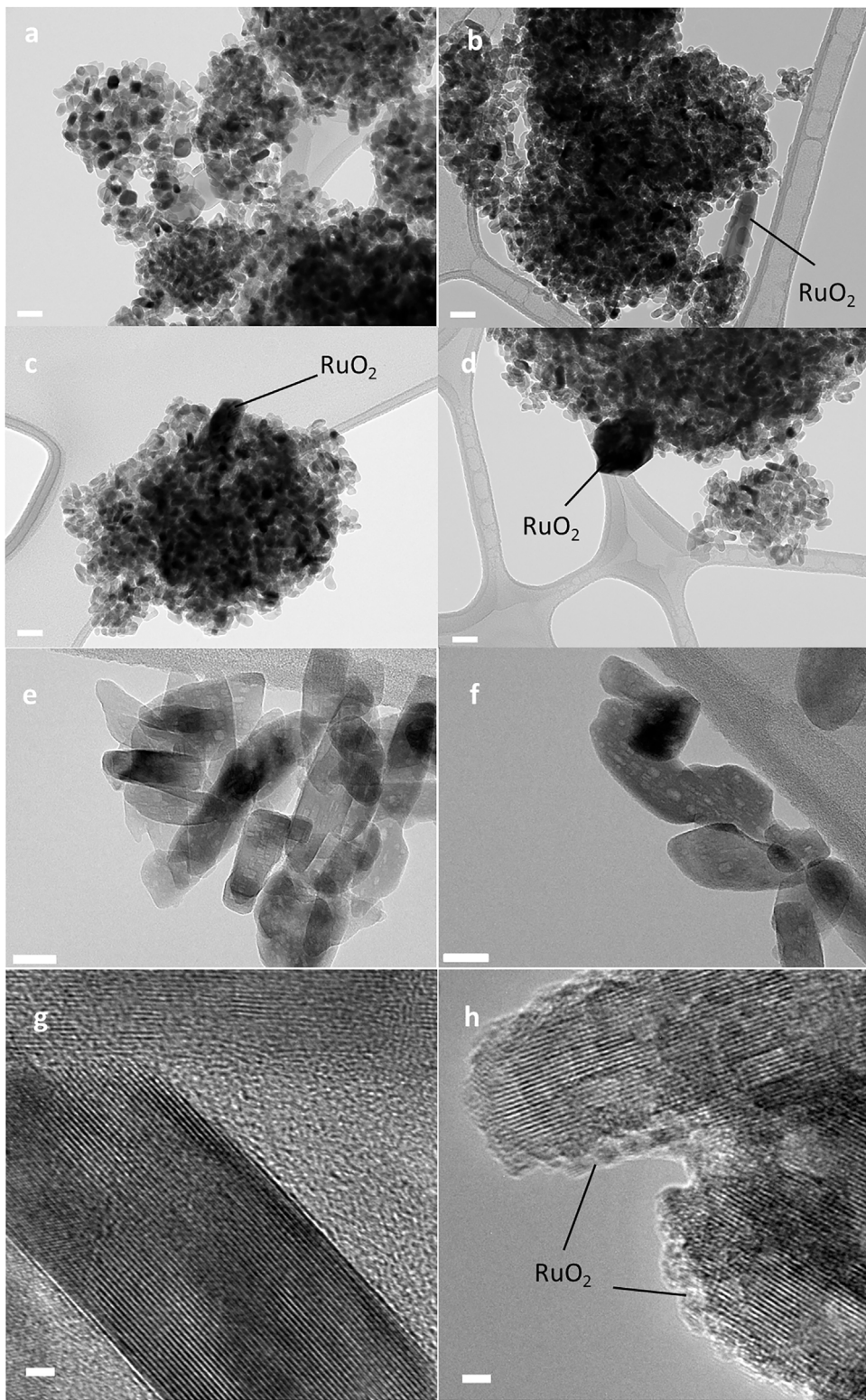


**Fig. 2.** TEM images of the RuO<sub>2</sub>/TiO<sub>2</sub> catalysts with different supports and synthesis methods. a: anatase TiO<sub>2</sub>; b: RuO<sub>2</sub>/anatase TiO<sub>2</sub>-WI; c: RuO<sub>2</sub>/anatase TiO<sub>2</sub>-DP; d: RuO<sub>2</sub>/anatase TiO<sub>2</sub>-SEA; e: rutile TiO<sub>2</sub>; f: RuO<sub>2</sub>/rutile TiO<sub>2</sub>-WI; g: HR-TEM of rutile TiO<sub>2</sub>; h: HR-TEM of RuO<sub>2</sub>/rutile TiO<sub>2</sub>-WI. Scale bars: a–d=50 nm; e–f=20 nm; g–h=2 nm.

as the ruthenium loading increased to 1 wt%. The impregnation of ruthenium onto rutile TiO<sub>2</sub> did not significantly decrease surface area or block the pores. For the synthesized SCR catalyst, the anatase TiO<sub>2</sub> support had a higher BET surface area than rutile TiO<sub>2</sub>, and the values measured were within a range of typical commercial SCR catalysts [42–45].

### 3.1.3. XRD

Both RuO<sub>2</sub>/anatase TiO<sub>2</sub>-WI and RuO<sub>2</sub>/rutile TiO<sub>2</sub>-WI catalysts were examined by XRD and the patterns are shown in Fig. 3. Other synthesis methods (DP and SEA) showed the same results as the WI method. The RuO<sub>2</sub>/anatase TiO<sub>2</sub> catalyst showed two additional RuO<sub>2</sub> peaks at  $2\theta = 28.0^\circ$  and  $35.1^\circ$  compared to pristine anatase

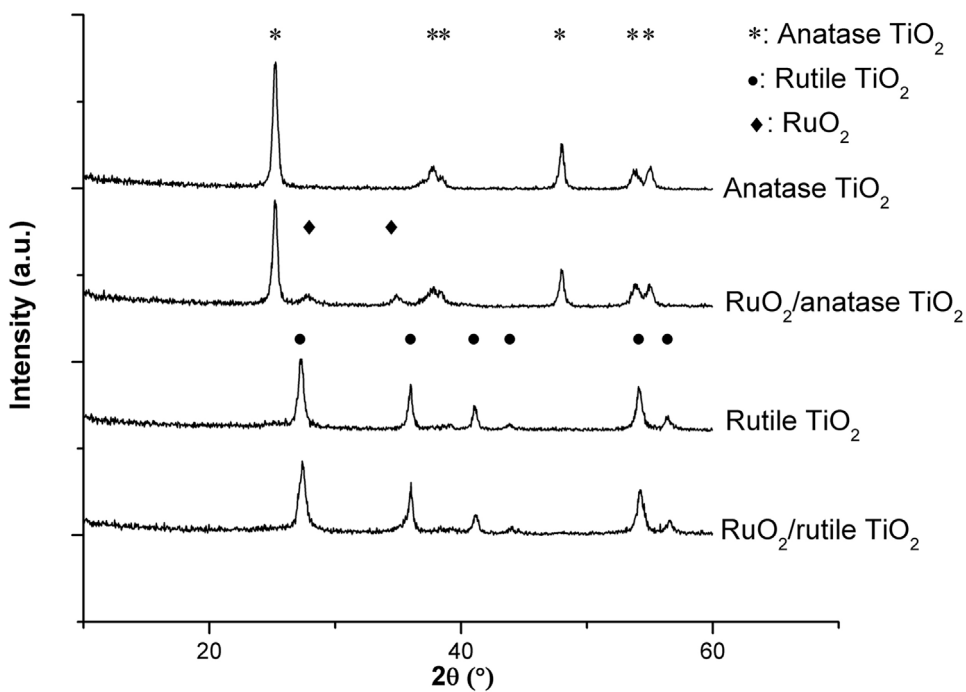


Fig. 3. XRD patterns of different  $\text{TiO}_2$  and  $\text{RuO}_2/\text{TiO}_2$ -WI catalysts.

$\text{TiO}_2$ . However, when rutile  $\text{TiO}_2$  was used as a support, no  $\text{RuO}_2$  could be detected. This result was consistent with the information obtained from the TEM results. On anatase  $\text{TiO}_2$ , the  $\text{RuO}_2$  crystal formation could be easily detected by XRD, while the nano-layers of  $\text{RuO}_2$  were formed on rutile  $\text{TiO}_2$ . For nano-structures, the local atom arrangements lack long-range 3-D periodicity that typical crystals have, making XRD nonideal for analyzing nanomaterials [46]. Therefore, an alternative characterization technique was needed to identify the ruthenium species on rutile  $\text{TiO}_2$ .

#### 3.1.4. XAFS

XAFS can give structural information of materials not affected by the state or morphology of the sample. Since XRD was unable to detect the  $\text{RuO}_2$  nano-layers formed on rutile  $\text{TiO}_2$ , XAFS was used to confirm the speciation of ruthenium.  $\text{RuO}_2$  catalysts supported on rutile  $\text{TiO}_2$  were used for the analysis. Ruthenium K edge (22,117 eV) XAFS spectra for the  $\text{RuO}_2/\text{rutile TiO}_2$  catalyst were collected. Since XAFS is an element-specific characterization technique,  $\text{TiO}_2$  in the catalyst does not interfere with the ruthenium measurement. The Fourier transformed spectra  $\chi(R)$  are shown in Fig. 4.  $\text{RuO}_2/\text{rutile TiO}_2$  catalysts with different synthesis methods showed the same result and only the result obtained from WI is shown here. Compared with a  $\text{RuO}_2$  standard, a fresh  $\text{RuO}_2/\text{rutile TiO}_2$  catalyst showed the same structure. The first major peak at around 1.5 Å is from a ruthenium atom and the neighboring oxygen atoms, and the second major peak at around 3.1 Å is from a center ruthenium atom and the neighboring ruthenium atoms. The spectra are similar to those reported in other studies [47,48]. The spectrum of the spent catalyst did not show any change, indicating that  $\text{RuO}_2$  was structurally stable under the simulated flue gas conditions.

### 3.2. $\text{Hg}(0)$ oxidation performances

#### 3.2.1. Effects of $\text{TiO}_2$ support and metal loading

The above catalyst characterization results showed major differences in morphology and dispersion of  $\text{RuO}_2$  on anatase and rutile  $\text{TiO}_2$  supports. Therefore,  $\text{Hg}(0)$  oxidation performances of 1 wt%

$\text{RuO}_2$  catalysts with different  $\text{TiO}_2$  supports and synthesis methods were evaluated and the results are shown in Fig. 5. Although the surface area of rutile  $\text{TiO}_2$  is slightly lower than anatase  $\text{TiO}_2$  under the same conditions, the  $\text{Hg}(0)$  oxidation performances of  $\text{RuO}_2/\text{rutile TiO}_2$  catalysts were around 70% higher than those of  $\text{RuO}_2/\text{anatase TiO}_2$  catalysts on average. When  $\text{RuO}_2$  was used as a Deacon catalyst for  $\text{HCl}$  oxidation, higher catalytic activity of  $\text{RuO}_2$  was reported over rutile  $\text{TiO}_2$  [32]. However, it is important to note that the different synthesis methods did not result in significant performance differences. These results are consistent with TEM images. The higher dispersion of  $\text{RuO}_2$  over rutile  $\text{TiO}_2$  due to lattice matching of these two very similar structures very likely leads to higher catalytic activity. Therefore, rutile  $\text{TiO}_2$  was chosen as a preferred substrate in this study, and WI was also selected as a preferred synthesis method because of its simplicity.

As a precious metal, a ruthenium loading on catalyst support should be optimized for the maximum utilization of the active metal. Therefore, the  $\text{RuO}_2/\text{rutile TiO}_2$  catalyst with different ruthenium loadings (0.2, 0.5 and 1 wt%) were compared (Fig. 6). In terms of the reaction rate of  $\text{Hg}(0)$  oxidized per mole of ruthenium used (i.e. turnover frequency), 0.5 wt% Ru loading gave the highest ruthenium utilization efficiency. The determination of  $\text{RuO}_2$  on  $\text{TiO}_2$  support using a chemisorption method has an inherent difficulty. It is well reported in the literature that the reduced form of  $\text{RuO}_2$  (i.e. Ru) becomes mobile and agglomerates on the  $\text{TiO}_2$  surface during the reduction step in chemisorption. This phenomena was reported by Komaya et al., and the attempts to eliminate the agglomeration by using different reduction conditions were not successful [49]. In this study, the determination of  $\text{RuO}_2$  dispersion over rutile the  $\text{TiO}_2$  phase was also attempted, but was not successful. Therefore, mass was used as a basis for the Ru loading instead of dispersion.

#### 3.2.2. Effects of temperature

When  $\text{RuO}_2$  was used as a Deacon catalyst, the activity was reported to be highest at around 400 °C [41]. This  $\text{RuO}_2/\text{rutile TiO}_2$   $\text{Hg}(0)$  oxidation catalyst can be located between the economizer and air preheater at coal-fired power plants. For power plants with a SCR unit, the catalyst can be located inside the SCR unit, or it can

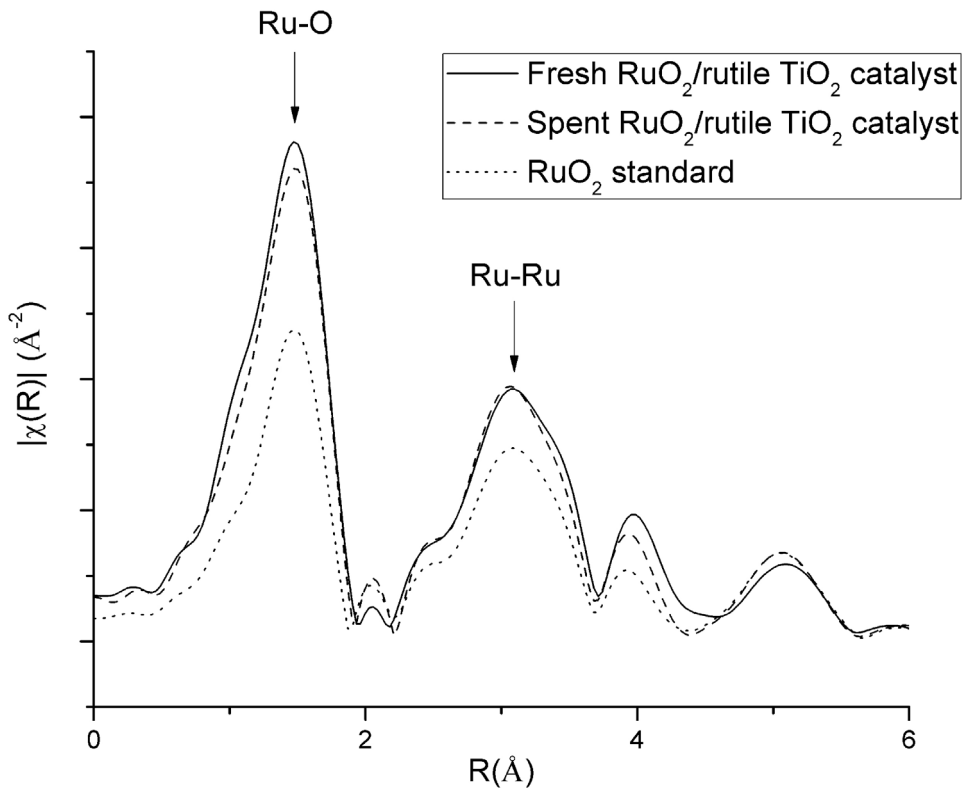


**Fig. 4.** Fourier transformed Ru XAFS spectra ( $|\chi(R)|$ ) for fresh  $\text{RuO}_2/\text{rutile TiO}_2$  catalyst, spent  $\text{RuO}_2/\text{rutile TiO}_2$  catalyst and  $\text{RuO}_2$  standard.

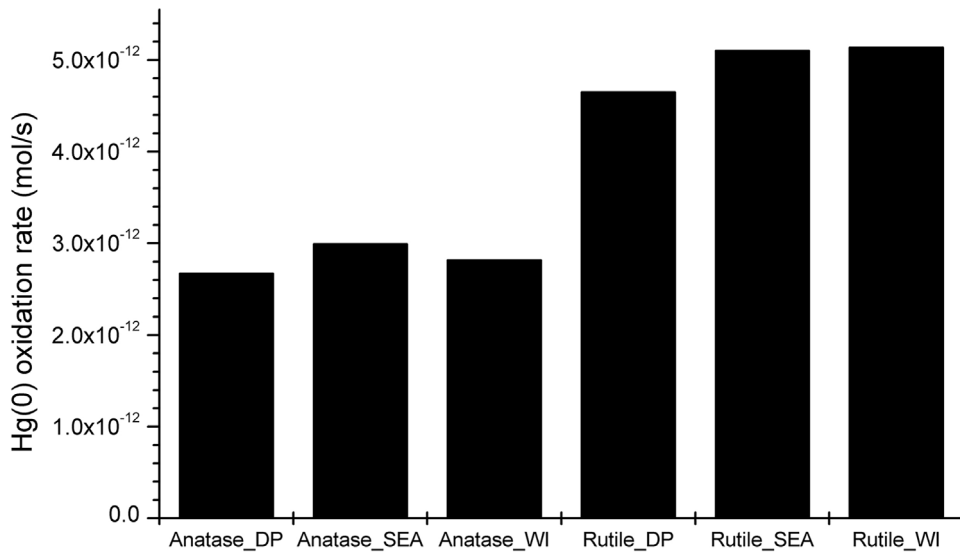


**Fig. 5.**  $\text{Hg}(0)$  oxidation activities of 1 wt%  $\text{RuO}_2/\text{TiO}_2$  catalysts with different  $\text{TiO}_2$  supports and synthesis methods. Conditions: 10 ppbv  $\text{Hg}(0)$ , 10 ppmv  $\text{HCl}$ , 3% (v)  $\text{O}_2$ , and balance  $\text{N}_2$  at  $T = 350^\circ\text{C}$ .

be a stand-alone unit before or after the SCR unit. 300–400 °C is an optimal temperature window for typical SCR catalysts when the boilers are at a full load [50]. The  $\text{RuO}_2/\text{rutile TiO}_2$   $\text{Hg}(0)$  oxidation catalyst can also utilize the same temperature window. The  $\text{Hg}(0)$  oxidation performances of  $\text{RuO}_2/\text{rutile TiO}_2$  catalyst at temperatures between 300 and 400 °C were evaluated as shown in Fig. 7. The results indicated that  $\text{RuO}_2/\text{rutile TiO}_2$  catalyst prefers higher temperature within the temperature window for  $\text{Hg}(0)$  oxidation.

### 3.2.3. $\text{Hg}(0)$ oxidation under simulated flue gases

For coal-fired power plants with SCR units for  $\text{NO}_x$  removal,  $\text{NH}_3$  as a reductant is injected into the front end of the SCR units. As the de- $\text{NO}_x$  reaction proceeds,  $\text{NH}_3$  concentration decreases along the SCR unit, and an  $\text{NH}_3$  slip at the tail end is usually controlled at <2 ppmv for commercial SCR catalysts [51]. The effect of  $\text{NH}_3$  gas on  $\text{Hg}(0)$  oxidation is shown in Fig. 8.  $\text{NH}_3$  has a strong inhibition effect on  $\text{Hg}(0)$  oxidation over  $\text{RuO}_2/\text{rutile TiO}_2$  catalyst. The catalyst lost almost all its  $\text{Hg}(0)$  oxidation capability when  $\text{NH}_3$  concentration

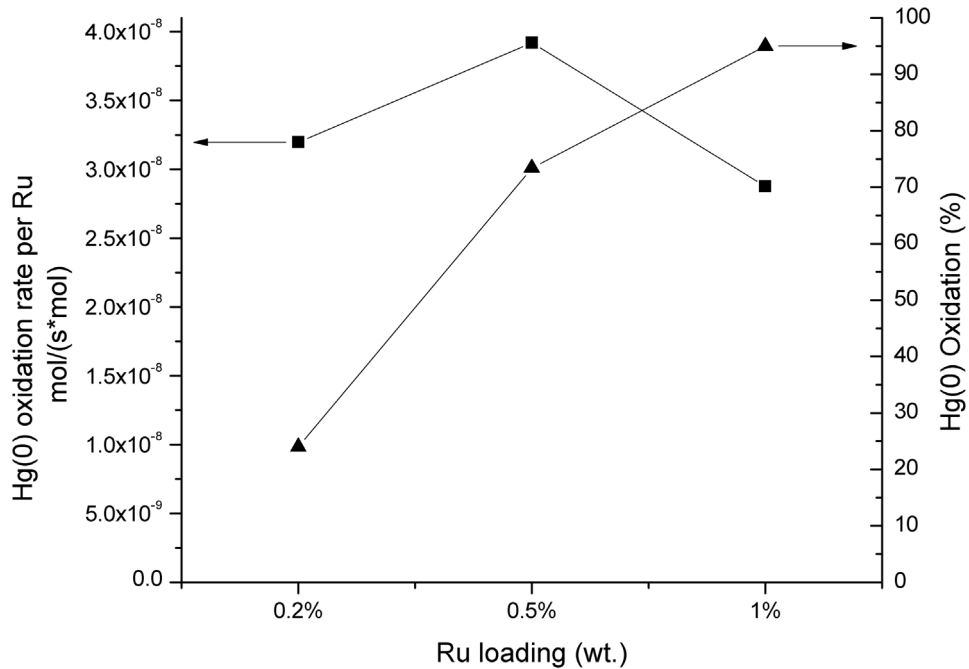


**Fig. 6.** Effect of metal loadings on the utilization efficiency of ruthenium on rutile  $\text{TiO}_2$  (WI method). Conditions: 10 ppbv  $\text{Hg}(0)$ , 10 ppmv  $\text{HCl}$ , 3%(v)  $\text{O}_2$ , and balance  $\text{N}_2$  at  $T=350^\circ\text{C}$ .

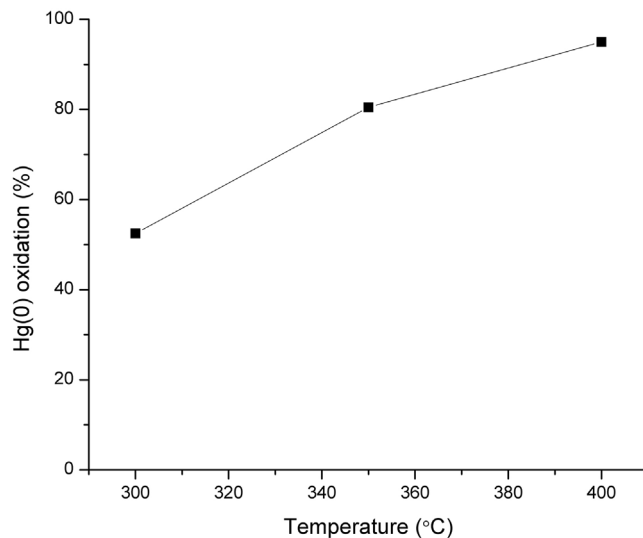


**Fig. 7.** Effect of temperature on the 1 wt%  $\text{RuO}_2$ /rutile  $\text{TiO}_2$ -WI catalyst activity. Conditions: 10 ppbv  $\text{Hg}(0)$ , 5 ppmv  $\text{HCl}$ , 3%(v)  $\text{O}_2$ , and balance  $\text{N}_2$ .

was increased to 50 ppmv. When the 50 ppmv  $\text{NH}_3$  was lowered back to 5 ppmv,  $\text{Hg}(0)$  oxidation was fully recovered. This corroborates that the adverse effect of  $\text{NH}_3$  is most likely derived from competitive adsorption with  $\text{HCl}$  onto active catalytic sites and not catalyst poisoning. Due to this limitation, the  $\text{RuO}_2$ /rutile  $\text{TiO}_2$  catalyst is not suitable for being located at the front end of a SCR unit. Installing at the tail end of a SCR unit, after the SCR unit, or for power plants without the SCR unit are possible options.

A  $\text{SO}_2$  concentration in a coal combustion flue gas greatly varies in terms of different types of coals with different sulfur contents. Generally, lignite and sub-bituminous coals have low  $\text{SO}_2$  (a few hundred ppmv in the flue gases) while bituminous coal has high  $\text{SO}_2$  (up to ~2,000 ppmv in the flue gas). The  $\text{Hg}(0)$  oxidation performances under different  $\text{SO}_2$  concentrations are shown in Fig. 9. It should be noted that these tests were carried out with only 10 ppmv

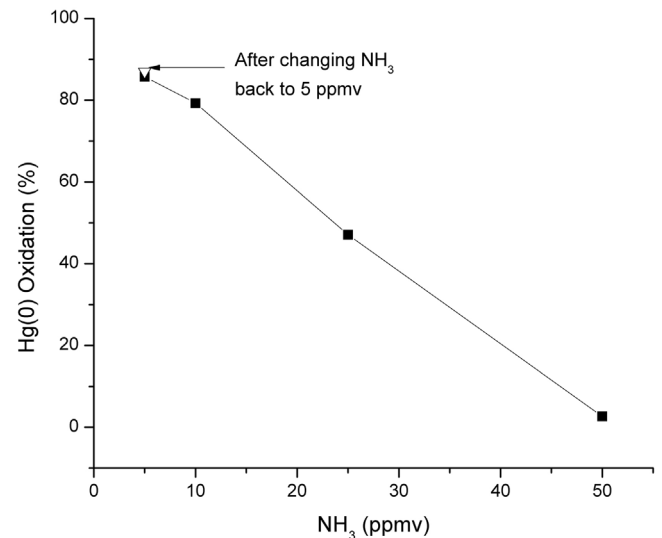


**Fig. 8.** Effect  $\text{NH}_3$  concentrations on  $\text{Hg}(0)$  oxidation performances of 1 wt%  $\text{RuO}_2$ /rutile  $\text{TiO}_2$ -WI catalyst under simulated flue gas. Conditions: 15 ppbv  $\text{Hg}(0)$ , 10 ppmv  $\text{HCl}$ , 5 ppmv  $\text{NO}$ , 200 ppmv  $\text{SO}_2$ , 3%(v)  $\text{O}_2$ , 10%(v)  $\text{H}_2\text{O}$ , 12%(v)  $\text{CO}_2$  balanced with  $\text{N}_2$  at  $350^\circ\text{C}$ .

$\text{HCl}$  just to demonstrate the effect of  $\text{SO}_2$  under extreme conditions. For bituminous coal flue gas with high  $\text{SO}_2$  concentration, the  $\text{HCl}$  concentration is also much higher (e.g., ~50–200 ppmv). Under such high  $\text{HCl}$  concentrations, the resistance of  $\text{Hg}(0)$  oxidation to  $\text{SO}_2$  is much lower as reported in our previous study [34]. In general, the  $\text{RuO}_2$ /rutile  $\text{TiO}_2$  catalyst has higher resistance to  $\text{SO}_2$  compared with other metal oxides-based catalysts such as  $\text{MnO}_2$  and  $\text{CeO}_2$  [52,53]. The  $\text{Hg}(0)$  oxidation performance was recovered when  $\text{SO}_2$  was lowered back to 200 ppmv, also indicating the competitive adsorption of  $\text{SO}_2$  with  $\text{HCl}$ . XRD analysis for the spent catalyst can be used to identify possible sulfates formation [54]. As shown in Fig. 10, the XRD diffraction pattern was consistent with that for the fresh  $\text{RuO}_2$ /rutile  $\text{TiO}_2$  catalyst (Fig. 3), and the

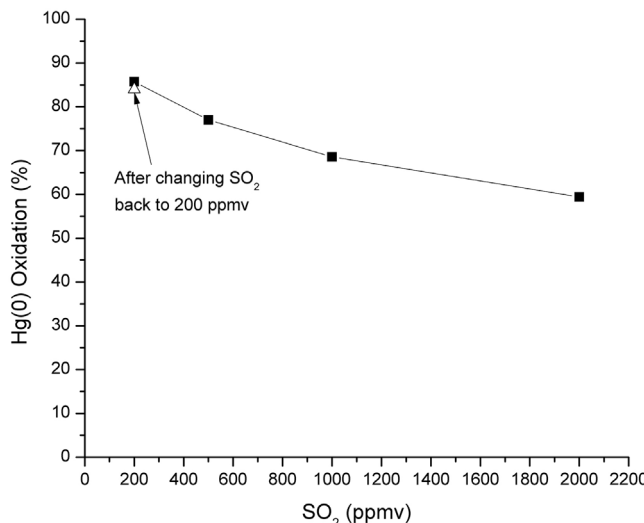


**Fig. 9.** Effect of SO<sub>2</sub> concentrations on Hg(0) oxidation performances of 1 wt% RuO<sub>2</sub>/rutile TiO<sub>2</sub>-WI catalyst under simulated flue gas. Conditions: 15 ppbv Hg(0), 10 ppmv HCl, 5 ppmv NH<sub>3</sub>, 5 ppmv NO, 3%(v) O<sub>2</sub>, 10%(v) H<sub>2</sub>O, 12%(v) CO<sub>2</sub> balanced with N<sub>2</sub> at 350 °C.

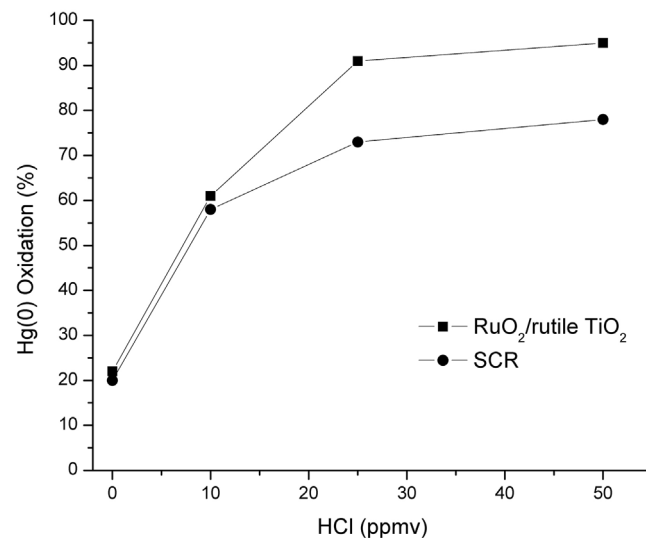


**Fig. 11.** Hg(0) oxidation performances of 1 wt% RuO<sub>2</sub>/rutile TiO<sub>2</sub>-WI catalyst with respect to different HCl concentration under a simulated flue gas condition of high sulfur bituminous coal. Conditions: 15 ppbv Hg(0), 5 ppmv NH<sub>3</sub>, 5 ppmv NO, 2,000 ppmv SO<sub>2</sub>, 3%(v) O<sub>2</sub>, 10%(v) H<sub>2</sub>O, 12%(v) CO<sub>2</sub> balanced with N<sub>2</sub> at 350 °C.

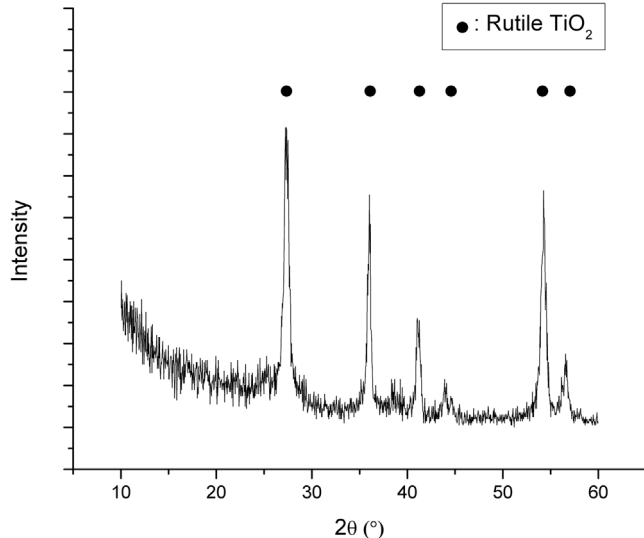


**Fig. 10.** XRD pattern of the spent RuO<sub>2</sub>/rutile TiO<sub>2</sub> catalyst. Conditions: 15 ppbv Hg(0), 10 ppmv HCl, 5 ppmv NH<sub>3</sub>, 5 ppmv NO, 200 ppmv SO<sub>2</sub>, 3%(v) O<sub>2</sub>, 10%(v) H<sub>2</sub>O, 12%(v) CO<sub>2</sub> balanced with N<sub>2</sub> at 350 °C for 48 h.

peaks for sulfate species were not observed. The XAFS analysis for the spent RuO<sub>2</sub>/rutile TiO<sub>2</sub> catalyst (Fig. 4) did not detect a formation of any potential bonding between ruthenium and sulfur. These results indicated that the catalyst was not poisoned by SO<sub>2</sub> during the reaction. Other flue gas components such as CO<sub>2</sub>, water vapor, and NO did not show any noticeable effect on Hg(0) oxidation over RuO<sub>2</sub>/rutile TiO<sub>2</sub> catalyst.

The Hg(0) oxidation performances of RuO<sub>2</sub>/rutile TiO<sub>2</sub> catalyst under simulated flue gas of sub-bituminous or lignite coal at the tail end of a SCR unit can be found in our previous paper [34]. The RuO<sub>2</sub>/rutile TiO<sub>2</sub> catalyst showed better Hg(0) oxidation performances than the SCR catalyst under all HCl concentrations. With only 10 ppmv HCl, the oxidation was >85%, and >90% could be achieved at 25 ppmv HCl under a typical simulated flue gas condition of low rank coal. For the scenario of bromine addition, HBr is at least 10 times more effective than HCl and >90% Hg(0) oxidation performance could be achieved with <1 ppmv HBr. Again, the

RuO<sub>2</sub>/rutile TiO<sub>2</sub> catalyst performed better than the SCR catalyst under all HBr concentrations.

Bituminous coal usually has high sulfur and chlorine contents with typical concentrations of ~1,000–2,000 ppmv SO<sub>2</sub> and ~50–200 ppmv HCl. Such high SO<sub>2</sub> concentrations usually significantly decrease the Hg(0) oxidation performances of most metal oxide-based catalysts [53,55,56]. The performance of the RuO<sub>2</sub>/rutile TiO<sub>2</sub> catalyst with a simulated flue gas containing 2,000 ppmv SO<sub>2</sub> is shown in Fig. 11. Although the Hg(0) oxidation performance at low HCl concentrations (e.g. <10 ppmv) decreased, >90% Hg(0) oxidation performances were obtained at a typical HCl concentration range (e.g. >50 ppmv) of bituminous coal. Overall, the RuO<sub>2</sub>/rutile TiO<sub>2</sub> catalyst has excellent Hg(0) oxidation performance and superior resistance to high SO<sub>2</sub>. One drawback of typical vanadium-based SCR catalysts is that V<sub>2</sub>O<sub>5</sub> can also oxidize SO<sub>2</sub> to SO<sub>3</sub>. The SO<sub>3</sub>/H<sub>2</sub>SO<sub>4</sub> emissions can cause corrosion problems and plume opacity especially when high sulfur coals are used. Therefore, the vanadium loading on SCR catalysts is limited by SO<sub>3</sub> generation and typical commercial SCR catalysts try to keep the SO<sub>2</sub> conversion below 1% [50]. The conversion was measured for the RuO<sub>2</sub>/rutile TiO<sub>2</sub> catalyst under the above simulated flue gas containing 2,000 ppmv SO<sub>2</sub>. It was found that only 0.17% of the SO<sub>2</sub> was oxidized to SO<sub>3</sub>, demonstrating another advantage of the RuO<sub>2</sub>/rutile TiO<sub>2</sub> catalyst under high sulfur conditions.

In our previous study, oxidized mercury species obtained from the RuO<sub>2</sub>/rutile TiO<sub>2</sub> catalyst were analyzed using XAFS [34]. In the presence of HCl or HBr gas, HgCl<sub>2</sub> or HgBr<sub>2</sub> was found to be the major oxidized mercury species. HgCl<sub>2</sub> and HgBr<sub>2</sub> have high solubility in water, and can be easily scrubbed by wet FGD scrubbers in coal-fired power plants.

#### 4. Conclusions

In this study, the RuO<sub>2</sub>/rutile TiO<sub>2</sub> catalyst for Hg(0) vapor oxidation was systematically studied in terms of different TiO<sub>2</sub> phases and synthesis methods for the first time. A combination of the two structurally similar components of RuO<sub>2</sub> as the active component and rutile TiO<sub>2</sub> as the support resulted in excellent RuO<sub>2</sub> dispersion over the rutile TiO<sub>2</sub> phase as opposed to anatase TiO<sub>2</sub> and thus high catalytic activity. The RuO<sub>2</sub> catalyst supported on rutile TiO<sub>2</sub> showed much higher Hg(0) oxidation activity than that on

anatase  $\text{TiO}_2$ . Among 0.2, 0.5, and 1 wt% Ru loadings, 0.5 wt% Ru loading onto rutile  $\text{TiO}_2$  gave the highest turnover frequency for  $\text{Hg}(0)$  oxidation. Different synthesis methods (WI, DP and SEA) did not show noticeable differences in the morphology or the activity of the  $\text{RuO}_2/\text{rutile TiO}_2$  catalyst. The  $\text{RuO}_2/\text{rutile TiO}_2$  catalyst performed well in a typical SCR temperature window of 350–400 °C and preferred higher temperature.  $\text{NH}_3$  and  $\text{SO}_2$  gases had negative effects on  $\text{Hg}(0)$  oxidation performances due to competitive adsorption with HCl. Between the two gases, the  $\text{RuO}_2/\text{rutile TiO}_2$  catalyst was more prone to  $\text{NH}_3$ . However, the catalyst showed very good  $\text{Hg}(0)$  oxidation performances under typical simulated flue gas conditions of sub-bituminous and lignite coals with low concentrations of HCl or HBr. It also showed excellent resistance to  $\text{SO}_2$  in comparison with a SCR catalyst under typical simulated flue gas conditions of high sulfur bituminous coal with up to 2,000 ppmv  $\text{SO}_2$ . It has potential for  $\text{Hg}(0)$  oxidation at the tail end section of the SCR unit in coal-fired power plants especially for high sulfur conditions where the catalytic activities of most metal oxide- or noble metal-based catalysts are significantly inhibited.

## Acknowledgements

This study was supported by the National Science Foundation, NSF CAREER Grant # 1151017, and Ohio Development Services Agency, Grant Agreement # OER-CDO-D-14-21. The authors greatly appreciate their financial support. Sector 9 facilities at the Advanced Photon Source of the Argonne National Laboratory, and research at these facilities, are supported by the U.S. Department of Energy – Basic Energy Sciences, the Canadian Light Source and its funding partners, and the Advanced Photon Source.

## References

- [1] L.J. Bragg, J.K. Oman, S.J. Tewalt, C.J. Oman, N.H. Rega, P.M. Washington, R.B. Finkelman, Analytical Data, Sample Locations, and Descriptive Information, Analytical Methods and Sampling Techniques, Database Perspective, and Bibliographic References for Selected U.S. Coal Samples: U.S Geological Survey Open-file Report 97–134, 1997.
- [2] B. Toole-O’Neil, S.J. Tewalt, R.B. Finkelman, D.J. Akers, Mercury concentration in coal—unraveling the puzzle, *Fuel* 78 (1999) 47–54.
- [3] US EPA. <https://www.epa.gov/mats/cleaner-power-plants#controls> (Accessed 7 September 2016).
- [4] National Emission Standards for Hazardous Air Pollutants From Coal- and Oil-Fired Electric Utility Steam Generating Units and Standards of Performance for Fossil-Fuel-Fired Electric Utility, Industrial-Commercial-Institutional, and Small Industrial-Commercial-Institutional Steam Generating Units. 40 CFR Parts 60 and 63. Federal Register 77:32 (Feb 16, 2012) p. 24976.
- [5] Federal Implementation Plans To Reduce Interstate Transport of Fine Particulate Matter and Ozone. 40 CFR Parts 51, 52, 72, 78, and 97. Federal Register 76 FR 48208, August 8, 2011.
- [6] C.L. Senior, S.A. Johnson, Impact of carbon-in-ash on mercury removal across particulate control devices in coal-fired power plants, *Energy Fuels* 19 (2005) 859–863.
- [7] R. Meij, The fate of mercury in coal-fired power plants and the influence of wet flue-gas desulphurization, *Water Air Soil Pollut.* 56 (1991) 21–33.
- [8] R. Meij, L.H.J. Vredenbregt, H.t. Winkel, The fate and behavior of mercury in coal-Fired power plants, *J. Air Waste Manage. Assoc.* 52 (2002) 912–917.
- [9] J.H. Pavlish, E.A. Sondreal, M.D. Mann, E.S. Olson, K.C. Galbreath, D.L. Laudal, S.A. Benson, Status review of mercury control options for coal-fired power plants, *Fuel Process. Technol.* 82 (2003) 89–165.
- [10] A.P. Jones, J.W. Hoffmann, D.N. Smith, T.J. Feeley, J.T. Murphy, DOE/NETL’s phase II mercury control technology field testing program: preliminary economic analysis of activated carbon injection, *Environ. Sci. Technol.* 41 (2007) 1365–1371.
- [11] S. Sjostrom, M. Durham, C.J. Bustard, C. Martin, Activated carbon injection for mercury control: overview, *Fuel* 89 (2010) 1320–1322.
- [12] Y. Zhao, M.D. Mann, J.H. Pavlish, B.A.F. Mibeck, G.E. Dunham, E.S. Olson, Application of gold catalyst for mercury oxidation by chlorine, *Environ. Sci. Technol.* 40 (2006) 1603–1608.
- [13] A.A. Presto, E.J. Granite, Noble metal catalysts for mercury oxidation in utility flue gas, *Platinum Met. Rev.* 52 (2008) 144–154.
- [14] P. Wang, S. Su, J. Xiang, F. Cao, L. Sun, S. Hu, S. Lei, Catalytic oxidation of  $\text{Hg}$  by  $\text{CuO}-\text{MnO}_2-\text{Fe 20}_3/\gamma-\text{Al}_2\text{O}_3$  catalyst, *Chem. Eng. J.* 225 (2013) 68–75.
- [15] W. Xu, H. Wang, X. Zhou, T. Zhu,  $\text{CuO}/\text{TiO}_2$  catalysts for gas-phase  $\text{Hg}$  0 catalytic oxidation, *Chem. Eng. J.* 243 (2014) 380–385.
- [16] H. Kamata, S.-i. Ueno, N. Sato, T. Naito, Mercury oxidation by hydrochloric acid over  $\text{TiO}_2$  supported metal oxide catalysts in coal combustion flue gas, *Fuel Process. Technol.* 90 (2009) 947–951.
- [17] N. Yan, W. Chen, J. Chen, Z. Qu, Y. Guo, S. Yang, J. Jia, Significance of  $\text{RuO}_2$  modified SCR catalyst for elemental mercury oxidation in coal-fired flue gas, *Environ. Sci. Technol.* 45 (2011) 5725–5730.
- [18] Y. Zhuang, J. Laumb, R. Liggett, M. Holmes, J. Pavlish, Impacts of acid gases on mercury oxidation across SCR catalyst, *Fuel Process. Technol.* 88 (2007) 929–934.
- [19] L. Zhao, C. Li, S. Li, Y. Wang, J. Zhang, T. Wang, G. Zeng, Simultaneous removal of elemental mercury and NO in simulated flue gas over  $\text{V}_2\text{O}_5/\text{ZrO}_2-\text{CeO}_2$  catalyst, *Appl. Catal. B: Environ.* 198 (2016) 420–430.
- [20] B.-A. Dranga, H. Koeser, Increased co-oxidation activity for mercury under hot and cold site coal power plant conditions—preparation and evaluation of  $\text{Au}/\text{TiO}_2$ -coated SCR-DeNO<sub>x</sub> catalysts, *Appl. Catal. B: Environ.* 166 (2015) 302–312.
- [21] H. Xu, Z. Qu, C. Zong, F. Quan, J. Mei, N. Yan, Catalytic oxidation and adsorption of  $\text{Hg}$  over low-temperature  $\text{NH}_3$ -SCR  $\text{LaMnO}_3$  perovskite oxide from flue gas, *Appl. Catal. B: Environ.* 186 (2016) 30–40.
- [22] H. Li, C.-Y. Wu, Y. Li, J. Zhang, Superior activity of  $\text{MnO}_x-\text{CeO}_2/\text{TiO}_2$  catalyst for catalytic oxidation of elemental mercury at low flue gas temperatures, *Appl. Catal. B: Environ.* 111–112 (2012) 381–388.
- [23] D. Jampaiah, K.M. Tur, P. Venkataswamy, S.J. Ippolito, Y.M. Sabri, J. Tardio, S.K. Bhargava, B.M. Reddy, Catalytic oxidation and adsorption of elemental mercury over nanostructured  $\text{CeO}_2-\text{MnO}_x$  catalyst, *RSC Adv.* 5 (2015) 30331–30341.
- [24] D. Jampaiah, S.J. Ippolito, Y.M. Sabri, B.M. Reddy, S.K. Bhargava, Highly efficient nanosized Mn and Fe codoped ceria-based solid solutions for elemental mercury removal at low flue gas temperatures, *Catal. Sci. Technol.* 5 (2015) 2913–2924.
- [25] J. Zhou, W. Hou, P. Qi, X. Gao, Z. Luo, K. Cen,  $\text{CeO}_2-\text{TiO}_2$  sorbents for the removal of elemental mercury from syngas, *Environ. Sci. Technol.* 47 (2013) 10056–10062.
- [26] J. He, G.K. Reddy, S.W. Thiel, P.G. Smirniotis, N.G. Pinto, Simultaneous removal of elemental mercury and NO from flue gas using  $\text{CeO}_2$  modified  $\text{MnO}_x/\text{TiO}_2$  materials, *Energy Fuels* 27 (2013) 4832–4839.
- [27] L. Zhao, C. Li, J. Zhang, X. Zhang, F. Zhan, J. Ma, Y.e. Xie, G. Zeng, Promotional effect of  $\text{CeO}_2$  modified support on  $\text{V}_2\text{O}_5-\text{WO}_3/\text{TiO}_2$  catalyst for elemental mercury oxidation in simulated coal-fired flue gas, *Fuel* 153 (2015) 361–369.
- [28] M.S. Berry, Full Scale Calcium Bromide Injection with Subsequent Mercury Oxidation and Removal Within Wet Flue Gas Desulphurization System: Experience at a 700 MW Coal-Fired Power Facility, The University of Alabama at Birmingham, 2012.
- [29] K. Dombrowski, S. McDowell, M. Berry, A.F. Sibley, R. Chang, B. Vosteen, The balance-of-plant impacts of calcium bromide injection as a mercury oxidation technology in power plants, in: Power Plant Air Pollutant Control Mega Symposium, Baltimore, MD, 2008.
- [30] Y. Zhuang, C. Chen, R. Timpe, J. Pavlish, Investigations on bromine corrosion associated with mercury control technologies in coal flue gas, *Fuel* 88 (2009) 1692–1697.
- [31] C.E. DiFrancesco, C.J. Bertole, J.T. Freeman, K. Nuchi, Achieving and maintaining Hg oxidation performance through SCR catalyst selection and management, in: Mega Symposium, Baltimore, MD, 2012.
- [32] K. Seki, Development of  $\text{RuO}_2/\text{rutile}-\text{TiO}_2$  catalyst for industrial HCl oxidation process, *Catal. Surv. Asia* 14 (2010) 168–175.
- [33] K. Iwanaga, K. Seki, T. Hibi, K. Issoh, T. Suzuta, M. Nakada, Y. Mori, T. Abe, The Development of Improved Hydrogen Chloride Oxidation Process, vol. 1, Sumitomo Kagaku, 2004.
- [34] Z. Liu, C. Li, V. Sriram, J.-Y. Lee, D. Brewe, XANES study of elemental mercury oxidation over  $\text{RuO}_2/\text{TiO}_2$  and selective catalytic reduction catalysts for mercury emissions control, *Fuel Process. Technol.* 153 (2016) 156–162.
- [35] V.P. Kumar, Y. Harikrishna, N. Nagaraju, K.V. Chary, Characterization and reactivity of  $\text{TiO}_2$  supported nano ruthenium catalysts for vapour phase hydrogenolysis of glycerol, *Indian J. Chem. A* 53 (2014) 516–523.
- [36] F. Pinna, Supported metal catalysts preparation, *Catal. Today* 41 (1998) 129–137.
- [37] L. Jiao, J.R. Regalbuto, The synthesis of highly dispersed noble and base metals on silica via strong electrostatic adsorption: I. Amorphous silica, *J. Catal.* 260 (2008) 329–341.
- [38] B. Ravel, M. Newville, ATHENA, ARTEMIS, HEPHAESTUS: data analysis for X-ray absorption spectroscopy using IFEFFIT, *J. Synchrotron Radiat.* 12 (2005) 537–541.
- [39] U.S. EPA Emission Measurement Center (EMC) of the Office of Air Quality Planning and Standards (OAQPS). Method 8: Determination of Sulfuric Acid and Sulfur Dioxide Emissions from Stationary Sources.
- [40] G. Xiang, X. Shi, Y. Wu, J. Zhuang, X. Wang, Size effects in atomic-level epitaxial redistribution process of  $\text{RuO}_2$  over  $\text{TiO}_2$ , *Sci. Rep.* 2 (2012).
- [41] M.A. Hevia, A.P. Amrute, T. Schmidt, J. Pérez-Ramírez, Transient mechanistic study of the gas-phase HCl oxidation to  $\text{Cl}_2$  on bulk and supported  $\text{RuO}_2$  catalysts, *J. Catal.* 276 (2010) 141–151.
- [42] Y. Eom, S.H. Jeon, T.A. Ngo, J. Kim, T.G. Lee, Heterogeneous mercury reaction on a selective catalytic reduction (SCR) catalyst, *Catal. Lett.* 121 (2008) 219–225.
- [43] H. Kamata, S.-i. Ueno, T. Naito, A. Yukimura, Mercury oxidation over the  $\text{V}_2\text{O}_5(\text{WO}_3)/\text{TiO}_2$  commercial SCR catalyst, *Ind. Eng. Chem. Res.* 47 (2008) 8136–8141.

[44] H. Kamata, K. Takahashi, C.U.I. Odenbrand, The role of  $K_2O$  in the selective reduction of NO with  $NH_3$  over a  $V_2O_5(WO_3)/TiO_2$  commercial selective catalytic reduction catalyst, *J. Mol. Catal. A: Chem.* 139 (1999) 189–198.

[45] Y. Zheng, A.D. Jensen, J.E. Johnsson, Laboratory investigation of selective catalytic reduction catalysts: deactivation by potassium compounds and catalyst regeneration, *Ind. Eng. Chem. Res.* 43 (2004) 941–947.

[46] B.S. Clausen, H. Topsøe, Application of combined X-Ray diffraction and absorption techniques, *Advances in Catalysis* 42 (1998) 315.

[47] Y.-Y. Hu, Z. Liu, K.-W. Nam, O.J. Borkiewicz, J. Cheng, X. Hua, M.T. Dunstan, X. Yu, K.M. Wiaderek, L.-S. Du, K.W. Chapman, P.J. Chupas, X.-Q. Yang, C.P. Grey, Origin of additional capacities in metal oxide lithium-ion battery electrodes, *Nat. Mater.* 12 (2013) 1130–1136.

[48] D.A. McKeown, P.L. Hagans, L.P. Carette, A.E. Russell, K.E. Swider, D.R. Rolison, Structure of hydrous ruthenium oxides: implications for charge storage, *J. Phys. Chem. B* 103 (1999) 4825–4832.

[49] T. Komaya, A.T. Bell, Z. Wengsiek, R. Gronsky, F. Engelke, T.S. King, M. Pruski, Effects of dispersion and metal–metal oxide interactions on Fischer–Tropsch synthesis over  $Ru/TiO_2$  and  $TiO_2$ -promoted  $Ru/SiO_2$ , *J. Catal.* 150 (1994) 400–406.

[50] P. Forzatti, Present status and perspectives in de- $NO_x$  SCR catalysis, *Appl. Catal. A: Gen.* 222 (2001) 221–236.

[51] Selective Catalytic Reduction (SCR) Control of  $NO_x$  Emissions From Fossil Fuel-Fired Electric Power Plants, Institute of Clean Air Companies (ICAC), 2009.

[52] H. Li, C.-Y. Wu, Y. Li, L. Li, Y. Zhao, J. Zhang, Role of flue gas components in mercury oxidation over  $TiO_2$  supported  $MnO_x$ – $CeO_2$  mixed-oxide at low temperature, *J. Hazard. Mater.* 243 (2012) 117–123.

[53] S. Qiao, J. Chen, J. Li, Z. Qu, P. Liu, N. Yan, J. Jia, Adsorption and catalytic oxidation of gaseous elemental mercury in flue gas over  $MnO_x$ /alumina, *Ind. Eng. Chem. Res.* 48 (2009) 3317–3322.

[54] Z. Zhou, X. Liu, Z. Liao, H. Shao, C. Lv, Y. Hu, M. Xu, Manganese doped  $CeO_2$ – $ZrO_2$  catalyst for elemental mercury oxidation at low temperature, *Fuel Process. Technol.* 152 (2016) 285–293.

[55] S. Eswaran, H.G. Stenger, Understanding mercury conversion in selective catalytic reduction (SCR) catalysts, *Energy Fuels* 19 (2005) 2328–2334.

[56] L. Ji, P.M. Sreekanth, P.G. Smirniotis, S.W. Thiel, N.G. Pinto, Manganese oxide/titania materials for removal of  $NO_x$  and elemental mercury from flue gas, *Energy Fuels* 22 (2008) 2299–2306.